

NASA/CR-1999-209514
ICASE Report No. 99-30



A Non-dissipative Staggered Fourth-order Accurate Explicit Finite Difference Scheme for the Time-domain Maxwell's Equations

Amir Yefet and Peter G. Petropoulos
New Jersey Institute of Technology, Newark, New Jersey

Institute for Computer Applications in Science and Engineering
NASA Langley Research Center
Hampton, VA

Operated by Universities Space Research Association



National Aeronautics and
Space Administration

Langley Research Center
Hampton, Virginia 23681-2199

Prepared for Langley Research Center
under Contract NAS1-97046

August 1999

A NON-DISSIPATIVE STAGGERED FOURTH-ORDER ACCURATE EXPLICIT FINITE DIFFERENCE SCHEME FOR THE TIME-DOMAIN MAXWELL'S EQUATIONS*

AMIR YEFET[†] AND PETER G. PETROPOULOS

Abstract. We consider a divergence-free non-dissipative fourth-order explicit staggered finite difference scheme for the hyperbolic Maxwell's equations. Special one-sided difference operators are derived in order to implement the scheme near metal boundaries and dielectric interfaces. Numerical results show the scheme is long-time stable, and is fourth-order convergent over complex domains that include dielectric interfaces and perfectly conducting surfaces. We also examine the scheme's behavior near metal surfaces that are not alligned with the grid axes, and compare its accuracy to that obtained by the Yee scheme.

Key words. Maxwell's equations, staggered schemes, finite differences, FD-TD scheme, explicit fourth-order schemes.

Subject classification. Applied Mathematics

1. Introduction. Recent engineering advances have resulted in ultra-wideband electromagnetic sources that find application in pulsed radar devices, ground-penetrating imaging systems, non-destructive evaluation of concrete structures, electronic on-chip interconnects, and novel communication systems. The need to simulate such problems requires fast and accurate solvers of the time-domain Maxwell's equations in complex open/closed domains filled with heterogeneous dielectrics in which metals may be embedded. A mini-review of how the Computational Electromagnetics (CEM) state of the art impacts such technologies can be found in [13]. For about a decade, Yee's Finite-Difference Time-Domain (FD-TD) algorithm [1] has provided the best [15] second-order accurate non-dissipative direct solution of the time-domain Maxwell's equations on a staggered grid. The numerical error is controlled solely by the mesh size, and the algorithm is particularly easy to implement in the presence of heterogeneous dielectrics and metal boundaries. As with all finite difference schemes, the algorithm is inherently dispersive and anisotropic [4] and, for large-scale problems or for problems requiring long-time integration of Maxwell's equations, errors from dispersion and anisotropy are significant unless the spatial discretization is extremely small [10]. This leads to prohibitive memory requirements and high computational cost when addressing realistic problems. For some time now, workers in CEM have realized the promise of high-order finite difference schemes. The question of staggered *vs.* collocated high-order schemes has been studied in [5] where it was shown that staggering is more efficient. At the same time a staggered high-order method can be constructed by altering a code that implements the staggered second-order accurate FD-TD algorithm. However, the extended spatial stencil of high-order methods has inhibited their wide acceptance as it does not allow for easy application of boundary conditions (absorbing, metal) and modeling of dielectric interfaces. The issue of implementing an absorbing layer in a promising staggered scheme that is fourth-order accurate in space and second-order accurate in time [12] has been addressed in [14]. It remained though that this particular high-order scheme (desirable due to its similarities to the Yee scheme) was only second-order convergent and slightly more accurate than FD-TD

*Supported in part by AFOSR Grant F49620-99-1-0072. Department of Mathematical Sciences, New Jersey Institute of Technology, University Heights, Newark, NJ 07102.

[†]This research was also supported by the National Aeronautics and Space Administration under NASA Contract No. NAS1-97046 while the author was in residence at the Institute for Computer Applications in Science and Engineering (ICASE), NASA Langley Research Center, Hampton, VA 23681-2199

when used to solve problems with metal boundaries and/or dielectric interfaces. In this paper we revisit the explicit non-dissipative staggered scheme presented in [12] in order to address the remaining objections to its use. We demonstrate that it is divergence-free, and propose a series of numerical boundary conditions, involving one-sided differentiation and extrapolation, to implement metal boundaries and dielectric interfaces. The treatment of dielectric interfaces herein is different from that in [11] where a simple pointwise specification of dielectric properties was used; we show in our Numerical Results section that such an approach degrades the global convergence rate of the scheme to second order. Also, the treatment of metal boundaries herein is different than that used in [10] where the method of images was applicable due to the infinite extend of those boundaries in the numerical test performed there. As shown in our Numerical Results section, these new numerical boundary conditions give almost the same results as the compact-implicit Ty(2,4) scheme [2], and (more importantly) preserve the fourth-order accuracy of the scheme. Together with the results on absorbing layers [14], the present paper should open the way towards a general acceptance of this scheme, which is an extension of Yee's algorithm to fourth-order accuracy. We now briefly outline the remainder of our paper. Section 2 describes the system of partial differential equations for which we will present the new boundary treatment for the fourth-order scheme considered herein. In Section 3 we present the details of the scheme and its numerical stability and accuracy properties; a derivation of the divergence-free property of the scheme is also given. Extensive numerical tests are given in Section 4; closed and open problems are considered and the actual convergence rate of a code based on the work herein is determined. In Section 5, we give a computational cost comparison between our approach and those of [1] and [2]. Section 6 closes the paper with a short discussion, conclusions drawn from the numerical experiments, and a description of future work required to turn this scheme into an engineering tool.

2. Preliminaries. The Maxwell equations in an isotropic non-dispersive medium are:

$$(2.1) \quad \begin{aligned} \nabla \times E + \frac{\partial B}{\partial t} &= 0 \quad (\text{Faraday's Law}), \\ -\nabla \times H + \frac{\partial D}{\partial t} &= 0 \quad (\text{Ampere's Law}), \end{aligned}$$

$$\begin{aligned} B &= \mu H, \\ D &= \epsilon E, \end{aligned}$$

coupled with Gauss's law

$$\begin{aligned} \nabla \cdot B &= 0 \\ \nabla \cdot D &= \rho. \end{aligned}$$

To simplify the notation we shall consider the two dimensional case, with the only sources for the problem being incident waves. These waves will be scattered after they encounter an obstacle. Furthermore, in free space, ϵ and μ are constants. The extension of the system of equations to three space dimensions, and the inclusion of sources and variable coefficients is straightforward. In two dimensions, the system (2.1) now decouples into two independent sets of equations. We shall consider the Transverse Magnetic (TM) set of equations where the electric field is a scalar while the magnetic field is a two-dimensional vector. Letting $\tau = ct = t/\sqrt{\mu\epsilon}$ and $Z = \sqrt{\frac{\mu}{\epsilon}}$, where ϵ and μ are the permittivity and permeability coefficients in free space, and c is the speed of light, the TM equations are:

$$\frac{\partial E_z}{\partial \tau} = Z \left(\frac{\partial H_y}{\partial x} - \frac{\partial H_x}{\partial y} \right)$$

$$(2.2) \quad \begin{aligned} \frac{\partial H_x}{\partial \tau} &= -\frac{1}{Z} \frac{\partial E_z}{\partial y} \\ \frac{\partial H_y}{\partial \tau} &= \frac{1}{Z} \frac{\partial E_z}{\partial x} \end{aligned}$$

3. The Scheme. The Yee scheme applied to (2.3) is

$$(3.1) \quad \begin{aligned} E_{z,i,j}^{n+1} &= E_{z,i,j}^n + Z \frac{\Delta \tau}{\Delta x} \delta_x H_{y,i,j}^{n+1/2} - Z \frac{\Delta \tau}{\Delta x} \delta_y H_{x,i,j}^{n+1/2} \\ H_{x,i,j-1/2}^{n+1/2} &= H_{x,i,j-1/2}^{n-1/2} - \frac{1}{Z} \frac{\Delta \tau}{\Delta y} \delta_y E_{z,i,j-1/2}^n \\ H_{y,i-1/2,j}^{n+1/2} &= H_{y,i-1/2,j}^{n-1/2} + \frac{1}{Z} \frac{\Delta \tau}{\Delta x} \delta_x E_{z,i-1/2,j}^n, \end{aligned}$$

where

Yee:

$$(3.2) \quad \begin{aligned} \delta_x U_{i,j} &= U_{i+1/2,j} - U_{i-1/2,j} \\ \delta_y U_{i,j} &= U_{i,j+1/2} - U_{i,j-1/2}. \end{aligned}$$

U is evaluated at the appropriate time and space location. In order to improve the accuracy of this scheme we replace the difference operators (3.2) by the following fourth-order accurate stencil for the spatial derivatives, e.g., $\frac{\partial U}{\partial y}$:

explicit(2,4):

$$(3.3) \quad \frac{\partial U}{\partial y}_{i,j+1/2} = \frac{1}{24\Delta y} (U_{i,j-1} - 27U_{i,j} + 27U_{i,j+1} - U_{i,j+2})$$

Hereafter we shall refer to (3.2) as the Yee scheme and to (3.3) as the explicit(2,4) scheme. To complete the fourth-order scheme at the first and last points of a bounded spatial domain we use fourth- and fifth-order accurate one sided approximations to the derivative. We note that this is used only in order to globally approximate the derivative. No physical boundary conditions are included at this stage. These one-sided approximations are as follows:

$$\begin{aligned} \frac{\partial U}{\partial y}_{i,1/2} &= \frac{1}{24\Delta y} (-22U_{i,0} + 17U_{i,1} + 9U_{i,2} - 5U_{i,3} + U_{i,4}) \\ \frac{\partial U}{\partial y}_{i,1} &= \frac{1}{24\Delta y} (-23U_{i,1/2} + 21U_{i,3/2} + 3U_{i,5/2} - U_{i,7/2}) \\ \frac{\partial U}{\partial y}_{i,N-1} &= \frac{1}{24\Delta y} (23U_{i,N-1/2} - 21U_{i,N-3/2} - 3U_{i,N-5/2} + U_{i,N-7/2}) \\ \frac{\partial U}{\partial y}_{i,N-1/2} &= \frac{1}{24\Delta y} (22U_{i,N} - 17U_{i,N-1} - 9U_{i,N-2} + 5U_{i,N-3} - U_{i,N-4}) \end{aligned}$$

We next define

$$(3.4) \quad \mathbf{A}_H = \frac{1}{24} \begin{bmatrix} -23 & 21 & 3 & -1 & . & . & 0 \\ 1 & -27 & 27 & -1 & . & . & 0 \\ 0 & 1 & -27 & 27 & -1 & . & 0 \\ . & . & . & . & . & . & . \\ 0 & . & . & 1 & -27 & 27 & -1 \\ 0 & . & . & 1 & -3 & -21 & 23 \end{bmatrix}.$$

$$(3.5) \quad \mathbf{A}_E = \frac{1}{24} \begin{bmatrix} -22 & 17 & 9 & -5 & 1 & \cdot & 0 \\ 1 & -27 & 27 & -1 & \cdot & \cdot & 0 \\ 0 & 1 & -27 & 27 & -1 & \cdot & 0 \\ \cdot & \cdot & \cdot & \cdot & \cdot & \cdot & \cdot \\ 0 & \cdot & \cdot & 1 & -27 & 27 & -1 \\ 0 & \cdot & -1 & 5 & -9 & -17 & 22 \end{bmatrix},$$

so the matrix form of the approximations to the derivative at the midpoint between grid points, and at the grid points is respectively:

$$\frac{\partial}{\partial y} \begin{bmatrix} U_{1/2} \\ U_{3/2} \\ \cdot \\ \cdot \\ U_{N-1/2} \end{bmatrix} = \frac{1}{24\Delta y} \mathbf{A}_E \begin{bmatrix} U_0 \\ U_1 \\ \cdot \\ U_{N-1} \\ U_N \end{bmatrix},$$

$$\frac{\partial}{\partial y} \begin{bmatrix} U_1 \\ U_2 \\ \cdot \\ \cdot \\ U_{N-1} \end{bmatrix} = \frac{1}{24\Delta y} \mathbf{A}_H \begin{bmatrix} U_{1/2} \\ U_{3/2} \\ \cdot \\ U_{N-3/2} \\ U_{N-1/2} \end{bmatrix}.$$

With these definitions, the matrix form of the discrete TM equations is:

$$[EZ_{i,j}]^{n+1} = [EZ_{i,j}]^n + \frac{\Delta t}{\Delta x} \mathbf{A}_H [\mathbf{H}Y_{i+1/2,j}]^{n+1/2} - \frac{\Delta t}{\Delta y} [\mathbf{H}X_{i,j+1/2}]^{n+1/2} \mathbf{A}_E^t$$

$$[\mathbf{H}X_{i,j+1/2}]^{n+1/2} = [\mathbf{H}X_{i,j+1/2}]^{n-1/2} - \frac{\Delta t}{\Delta y} [EZ_{i,j}]^n \mathbf{A}_E^t$$

$$[\mathbf{H}Y_{i+1/2,j}]^{n+1/2} = [\mathbf{H}Y_{i+1/2,j}]^{n-1/2} - \frac{\Delta t}{\Delta x} \mathbf{A}_E [\mathbf{E}Z_{i,j}]^n.$$

Note, the staggering in time and space results in a scheme that is second-order accurate in time and fourth-order accurate in space.

3.1. Divergence of Computed Fields. We now demonstrate that the explicit (2,4) scheme is divergence-free for TM waves, that is

$$\frac{\partial}{\partial t} \text{div}(\mu H_x, \mu H_y) = 0.$$

We note that μ may be a function of the spatial variables and introduce the relations:

$$[(\mu HX)_{i,j+1/2}]^{n+1/2} = [(\mu HX)_{i,j+1/2}]^{n-1/2} - \frac{\Delta t}{\Delta y} [EZ_{i,j}]^n \mathbf{A}_E^t$$

$$[(\mu HY)_{i+1/2,j}]^{n+1/2} = [(\mu HY)_{i+1/2,j}]^{n-1/2} - \frac{\Delta t}{\Delta x} \mathbf{A}_E [\mathbf{E} \mathbf{Z}_{i,j}]^n.$$

Multiplying the first equation above by $1/\Delta x$ and \mathbf{A}_E , the second equation by $1/\Delta y$ and \mathbf{A}_E^t , and adding we get

$$\begin{aligned} & \left(\frac{1}{\Delta x} \mathbf{A}_E [(\mu \mathbf{H} \mathbf{X})_{i,j+1/2}] + \frac{1}{\Delta y} [(\mu \mathbf{H} \mathbf{Y})_{i+1/2,j}] \mathbf{A}_E^t \right)^{n+1} = \\ & \left(\frac{1}{\Delta x} \mathbf{A}_E [(\mu \mathbf{H} \mathbf{X})_{i,j+1/2}] + \frac{1}{\Delta y} [(\mu \mathbf{H} \mathbf{Y})_{i+1/2,j}] \mathbf{A}_E^t \right)^n. \end{aligned}$$

Hence, if the field is numerically divergence-free initially it will remain so ever after. If the μ is discontinuous then the derivation of the property differs. In that case we segment the domain into subdomains, and on the boundaries of the dielectric we use a fourth-order extension of the approach developed for second-order schemes in [6] and [7]. The details of the fourth-order extension to handle dielectric interfaces is given in Section 4.

3.2. Time Step. For each of the methods described above one must choose a time step for the numerical integration. This time step is based on two considerations: stability and accuracy. Since all the schemes have stability limits, this places an upper bound on the usable time step.

The amplification factor is given by:

$$\sigma_{leapfrog} = 1 + \frac{1}{2} z^2 \pm \sqrt{\left(1 + \frac{1}{2} z^2\right)^2 - 1}$$

$z = \lambda \Delta t$. λ is an eigenvalue of the Fourier transform of the spatial approximation. Let $D = \left[\frac{1}{(\Delta x)^2} + \frac{1}{(\Delta y)^2} \right]^{1/2}$. Then

$$|\lambda_{explicit}| = \frac{1}{12} \left(\frac{[27 \sin(\frac{\theta}{2}) - \sin(\frac{3\theta}{2})]^2}{(\Delta x)^2} + \frac{[27 \sin(\frac{\phi}{2}) - \sin(\frac{3\phi}{2})]^2}{(\Delta y)^2} \right)^{1/2} \leq \frac{7}{3} D$$

Since we wish to obtain higher order accuracy it is also necessary to limit the time-step by accuracy requirements. We do not want the accuracy of the scheme to be determined by the time integration. Hence, the temporal error should be equal to or less than the spatial error. For the Yee scheme one should choose the time step close to the stability limit. For the explicit(2,4) scheme the time step chosen depends on the accuracy desired. As the mesh is refined the spatial error decreases as of a fourth order scheme and so decreases faster than the temporal error. Thus, the time step should depend on $(\Delta x)^2$. If the error requirements are too severe then this is inefficient and the leapfrog in time should be replaced by a fourth order Runge-Kutta method. However, for the experiments in this paper we shall use the same leapfrog method for both schemes.

3.3. Spatial Accuracy. There are several ways of constructing fourth order methods. We can use either a staggered mesh or locate all the variables at the same mesh point. In addition we can either use a five point stencil in each direction to approximate the first derivative or else use a three point stencil with an implicit matrix inversion. Define the following operators:

- $D_0 u = \frac{u_{j+1/2} - u_{j-1/2}}{h}$

- $D_1 u = \frac{(u_{j-3/2} - u_{j+3/2}) + 27(u_{j+1/2} - u_{j-1/2})}{24h}$
- $\frac{(D_2 u)_{j+1} + (D_4 u)_{j-1}}{24} + \frac{11}{12}(D_4 u)_j = \frac{u_{j+1/2} - u_{j-1/2}}{h}$

We define the truncation error as $T = Du - \frac{du}{dx} = \tau h^4$. By a Taylor series expansion we get

- $\tau_1 = \frac{3}{640} \sim .0046875$
- $\tau_2 = \frac{17}{5760} \sim .00295$

Kreiss and Olinger [3] give a simple analysis, for semi-discrete approximations, to calculate the number of points per wavelength needed to resolve a wave with speed a and given accuracy ϵ . Let ω be the wave number ($u(x, t) = e^{i\omega x - at}$). We consider the solution over q periods so that $t = \frac{2\pi q}{\omega a}$. They find that the number of points per wavelength, M , needed for accuracy ϵ is given by

$$M = 2\pi(2\pi\tau)^{1/p} \left(\frac{q}{\epsilon}\right)^{1/p},$$

where p is the order of the scheme.

If we choose $\epsilon = .01$, one percent error, then we get

- $M_0 \sim 32.15q^{1/2}$
- $M_1 \sim 8.23q^{1/4}$
- $M_2 \sim 7.33q^{1/4}$

As seen from the formulas of Kreiss and Olinger the benefits of a fourth order method, compared with a second order method, improve as one demands higher accuracy (e.g. 0.1 %) and with longer times of integration. We conclude that either staggering or a compact implicit method gives substantial improvement over the simplest fourth order accurate method. Combining staggering with an implicit method gives a little more improvement (see also [5]). We stress that staggering also helps in the imposition of the boundary conditions. In addition using the Yee placement of the variables simplifies the conversion of an existing code to fourth order accuracy.

If one assumes a uniform grid-spacing, i.e. $\Delta x = \Delta y = h$, and defines the number of points per wavelength to be $N = \frac{2\pi}{kh}$, then the numerical wave speed c^* can be written as:

$$\begin{aligned} c_{Yee}^* &= \frac{N}{\pi} \left[\sin^2\left(\frac{\pi \cos(\theta)}{N}\right) + \sin^2\left(\frac{\pi \sin(\theta)}{N}\right) \right]^{1/2} \\ c_{explicit}^* &= \frac{N}{24\pi} \left(\left[27 \sin\left(\frac{\pi \cos(\theta)}{N}\right) - \sin\left(\frac{3\pi \cos(\theta)}{N}\right) \right]^2 \right. \\ &\quad \left. + \left[27 \sin\left(\frac{\pi \sin(\theta)}{N}\right) - \sin\left(\frac{3\pi \sin(\theta)}{N}\right) \right]^2 \right)^{1/2} \end{aligned}$$

Shown in Fig. 3.1 are the polar diagrams of the numerical phase speed for $N = 1, 2, 4, 8$ and 16 for the two schemes. A comparison of the numerical phase speed for $N = 20$ is given in Fig. 3.2. The numerical phase speed in the two schemes experiences a phase lag. The lag decreases as N increases. The lag decreases for the explicit scheme. In other words, for a given grid-spacing, the error $(1 - c^*)$ for high frequency modes is greater than that for low frequency modes. For a fixed N , the error using Yee's scheme is greater than The explicit. The two figures also demonstrate the anisotropy inherent in the discretizations.

One observes that the error is the greatest along the axes ($\theta = 0, \pi/2, \pi$ and $3\pi/2$) and the least along the diagonals ($\theta = \pi/4, 3\pi/4, 5\pi/4$ and $7\pi/4$). An important quantity to measure is the isotropy error defined as the difference of the maximum and the minimum values of the numerical phase speed. For $N=20$, as shown in Fig. 3.2 the isotropy errors are 0.2% for the Yee scheme and 0.0034% in for the explicit scheme.

Expanding c^* one obtains the error:

$$1 - c_{Yee}^* = \frac{\pi^2}{N^2} \left(\frac{1}{8} + \frac{1}{24} \cos(4\theta) \right)$$

$$1 - c_{explicit}^* = \frac{3\pi^4}{320N^4} (5 + 3\cos(4\theta))$$

The above equation shows that the leading dispersive errors in Yee's scheme is inversely proportional to N^2 and in the explicit scheme is inversely proportional to N^4 . This, of course, is just a reflection that Yee's scheme is second order accurate in space while the explicit scheme is fourth order accurate in space. It also shows that the leading dispersive error is a function of the wave propagation direction θ on each grid.

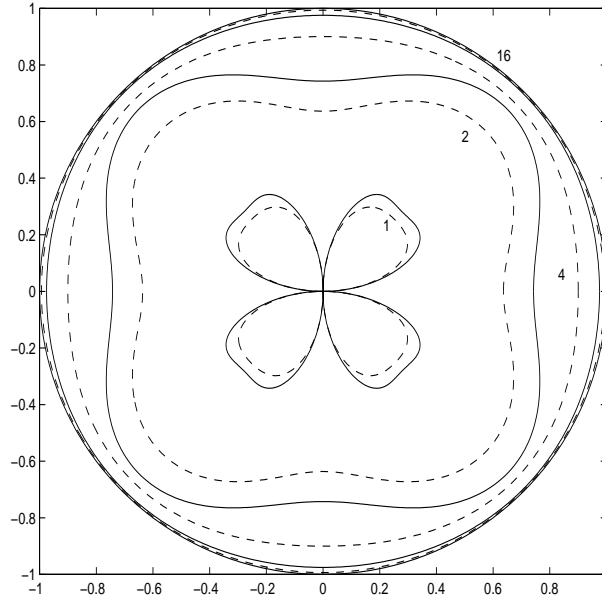


FIG. 3.1. Polar diagram of the numerical phase speed. Yee:—, explicit(2,4):-.

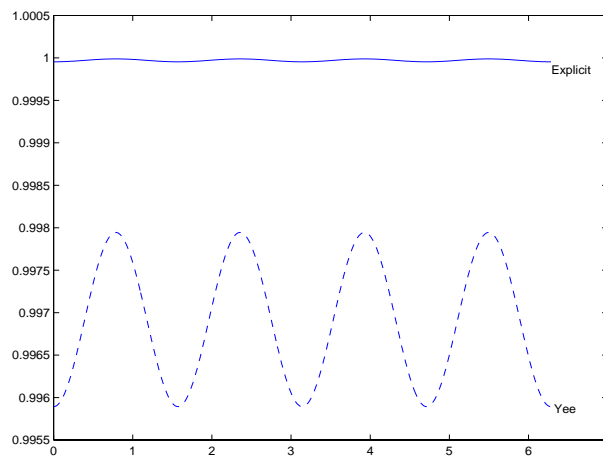


FIG. 3.2. Comparison of numerical phase speed, $0 \leq \theta \leq 2\pi$.

3.4. Numerical Errors of Spatial and Time Discretization. We have discussed spatial and time errors individually in the previous sections. In this section we will investigate the numerical errors from the

combined discretization. These errors can be determined from the eigenvalues of the amplification matrix. In Fig. 3.3 the curves labeled 'exact' are the normalized phase shift using the exact time integration. The difference between these curves and the value 1 is the spatial phase error, which can have either a phase lag or a phase lead. The other curves are the normalized phase shift using the staggered leapfrog (with Yee and the explicit(2,4)) with $CFL = \frac{1}{2}$. For the Yee scheme the difference between each curve and the exact curve is an additional phase error due to time discretization. Leapfrog has a larger error and a phase lead and so moves the curve away from 1. Except for a very small contribution due to the nonlinear relation between σ and λ , the time discretization does not reduce the isotropy error introduced by the spatial discretization.

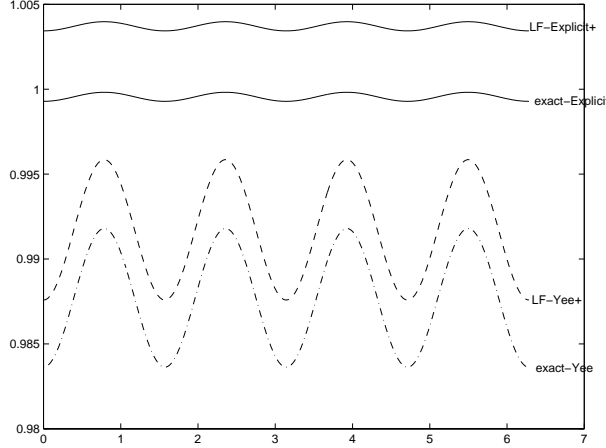


FIG. 3.3. Comparison of phase shifts for complete discretization.

4. Computational Results. In this section we compare three different schemes: the standard Yee scheme, the explicit(2,4) scheme as extended herein, and the Ty(2,4) [2] scheme. All schemes are advanced in time by the leapfrog method. For all computations we choose $Z = 1$. For the numerical examples that are posed in an open domain we use a PML method in the far field. In all cases the error is measured against the exact E_z in the L_2 norm. All numerical examples herein test the accuracy and stability of the one-sided differencing and extrapolation operators introduced in Section 2 and in the present Section.

We first consider a test case with the following initial and boundary conditions:

$$\begin{aligned} E_z &= \sin(3\pi x) \sin(4\pi y) \\ H_y &= (3/5) \cos(3\pi x) \sin(4\pi y) \sin\left(\frac{5\pi\Delta t}{2}\right) \\ H_x &= -(4/5) \sin(3\pi x) \cos(4\pi y) \sin\left(\frac{5\pi\Delta t}{2}\right) \end{aligned}$$

The exact solution in this case is:

$$E_z = \sin(3\pi x) \sin(4\pi y) \cos(5\pi t)$$

For the three schemes we choose uniform grid spacing. For the Yee, the explicit(2,4) and the Ty(2,4) schemes we take: $h = \Delta x = \Delta y = 1/20, 1/40, 1/80$. For the Yee scheme we set $\Delta t = 2h/3$, while for the explicit(2,4) and Ty(2,4) schemes we set $\Delta t = h^2$. Figures 4.1a-4.1c show the actual logarithmic errors as a function of time. Figure 4.1d shows the convergence rate of the L_2 spatial error in the maximum norm over the time interval $[0, 10]$. The slope of the line for the Yee scheme converges to 2, and the slope of the lines for both the explicit(2,4) and Ty(2,4) schemes converge to 4. This can also be seen in Table 4.1.

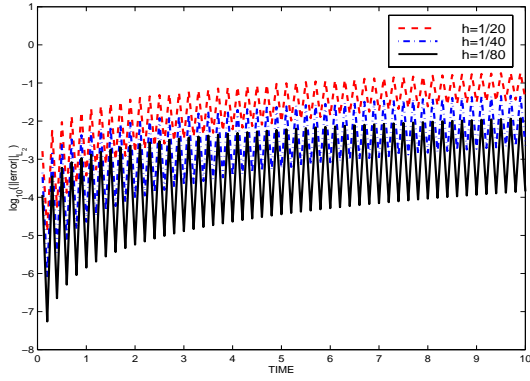


FIG. 4.1A. $\log_{10}(\|error\|_{L_2})$ For the Yee scheme.

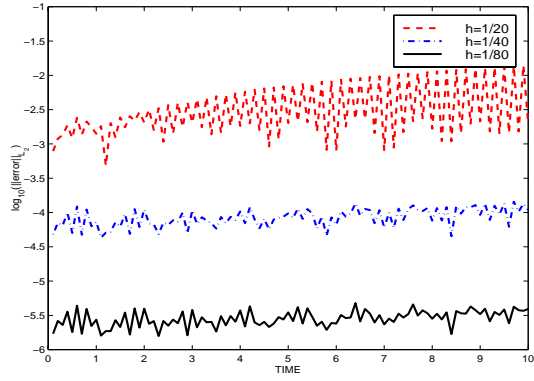


FIG. 4.1B. $\log_{10}(\|error\|_{L_2})$ for the explicit(2,4) scheme.

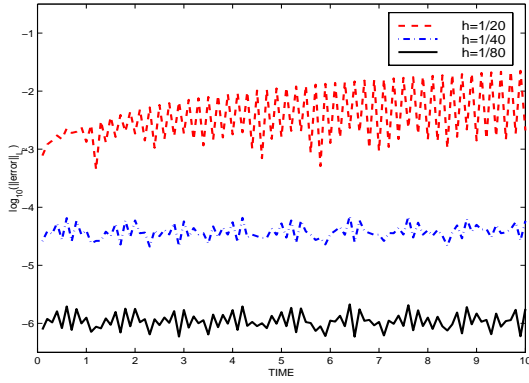


FIG. 4.1C. $\log_{10}(\|error\|_{L_2})$ for the Ty(2,4) scheme.

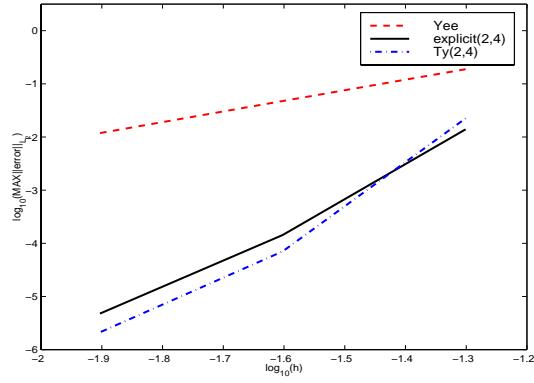


FIG. 4.1D. $\text{Log}_{10}(\|error\|_{L_2})$ as a function of $\text{Log}_{10}(h)$ For the Yee, the explicit(2,4) and the Ty(2,4) schemes.

TABLE 4.1

The maximal errors in L_2 norm for each mesh size

scheme	h	Δt	$Max(\ error\ _{L_2})$ $0 \leq t \leq 10$	rate
explicit(2,4)	$\frac{1}{20}$	$\frac{1}{400}$	0.014	
explicit(2,4)	$\frac{1}{40}$	$\frac{1}{1600}$	1.43×10^{-4}	6.60
explicit(2,4)	$\frac{1}{80}$	$\frac{1}{3200}$	4.76×10^{-6}	4.9152
Ty(2,4)	$\frac{1}{20}$	$\frac{1}{400}$	0.0224	
Ty(2,4)	$\frac{1}{40}$	$\frac{1}{1440}$	7.07×10^{-5}	8.306
Ty(2,4)	$\frac{1}{80}$	$\frac{1}{3440}$	2.12×10^{-6}	5.0589
Yee	$\frac{1}{20}$	$\frac{1}{35}$	0.189	
Yee	$\frac{1}{40}$	$\frac{1}{70}$	0.0475	1.99
Yee	$\frac{1}{80}$	$\frac{1}{140}$	0.0118	2.003

We next consider the simplest mode of propagation in a rectangular cross section wave guide. We take

the walls to be perfect conductors. We take the following boundary and initial conditions:

$$\begin{aligned}
 E_z(x, y, 0) &= \sin(3\pi x) \sin(4\pi y) \\
 H_y(x, y, \frac{\Delta t}{2}) &= -\frac{3}{5} \sin(3\pi x - \frac{5\pi\Delta t}{2}) \sin(4\pi y) \\
 H_x(x, y, \frac{\Delta t}{2}) &= -\frac{4}{5} \cos(3\pi x - \frac{5\pi\Delta t}{2}) \sin(4\pi y) \\
 E_z(0, y, t) &= -\sin(5\pi t) \sin(4\pi y) \\
 E_z(1, y, t) &= \sin(3\pi - 5\pi t) \sin(4\pi y) \\
 E_z(x, 0, t) &= 0 \\
 E_z(x, 1, t) &= 0
 \end{aligned}$$

The solution is then:

$$E_z(x, y, t) = \sin(3\pi x - 5\pi t) \sin(4\pi y).$$

For the three schemes we choose uniform grid spacing. For the Yee, the explicit(2,4), and the Ty(2,4) schemes we again take: $h = \Delta x = \Delta y = 1/20, 1/40, 1/80$. The CFL numbers are chosen as before. In the figure 4.2d we draw the error as a function of the mesh size. For this test problem too the slope for the Yee scheme converges to 2 while that for the explicit(2,4) converges to 4. In table 4.2 we present the errors in L_2 norm for the Yee and the explicit(2,4) scheme. In both cases the errors are almost linear in time. However as the mesh is refined the Yee scheme yields second order accuracy while the explicit(2,4) yields between fourth and fifth order accuracy.

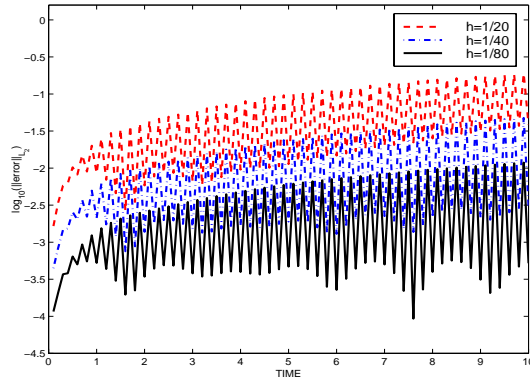


FIG. 4.2A. $\log_{10}(\|error\|_{L_2})$ For the Yee scheme.

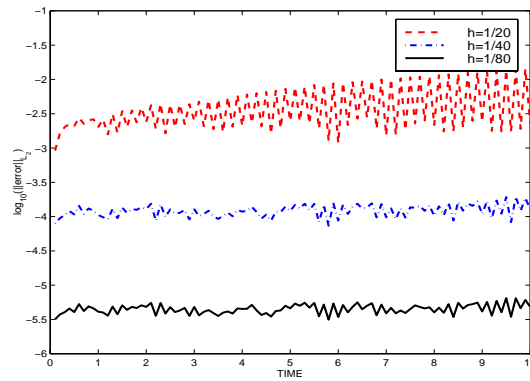


FIG. 4.2B. $\log_{10}(\|error\|_{L_2})$ For the explicit(2,4) scheme.

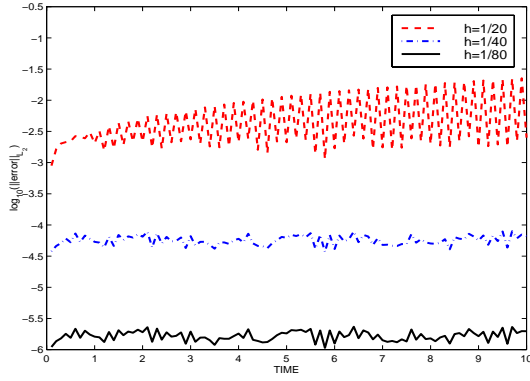


FIG. 4.2C. $\log_{10}(\|error\|_{L_2})$ For the $Ty(2,4)$ scheme.

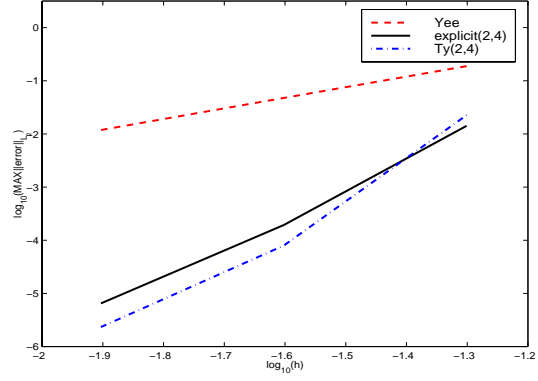


FIG. 4.2D. $\log_{10}(\|error\|_{L_2})$ as a function of $\log_{10}(h)$ For the Yee, the explicit(2,4) and the $Ty(2,4)$ schemes.

TABLE 4.2
The maximal errors in L_2 norm.

<i>scheme</i>	h	Δt	$Max(\ error\ _{L_2})$ $0 \leq t \leq 10$	<i>rate</i>
<i>explicit(2,4)</i>	$\frac{1}{20}$	$\frac{1}{400}$	0.014	
<i>explicit(2,4)</i>	$\frac{1}{40}$	$\frac{1}{1600}$	1.9316×10^{-4}	6.2
<i>explicit(2,4)</i>	$\frac{1}{80}$	$\frac{1}{3200}$	6.48×10^{-6}	4.896
<i>Ty(2,4)</i>	$\frac{1}{20}$	$\frac{1}{400}$	0.0242	
<i>Ty(2,4)</i>	$\frac{1}{40}$	$\frac{1}{1440}$	7.9304×10^{-5}	8.15
<i>Ty(2,4)</i>	$\frac{1}{80}$	$\frac{1}{3440}$	2.329×10^{-6}	5.089
<i>Yee</i>	$\frac{1}{20}$	$\frac{1}{30}$	0.1889	
<i>Yee</i>	$\frac{1}{40}$	$\frac{1}{60}$	0.0476	1.9885
<i>Yee</i>	$\frac{1}{80}$	$\frac{1}{120}$	0.0119	2.0032

We next consider the treatment of a domain which contains air and a lossless dielectric with a relative permittivity of ϵ_2 as shown in Figure 4.3.

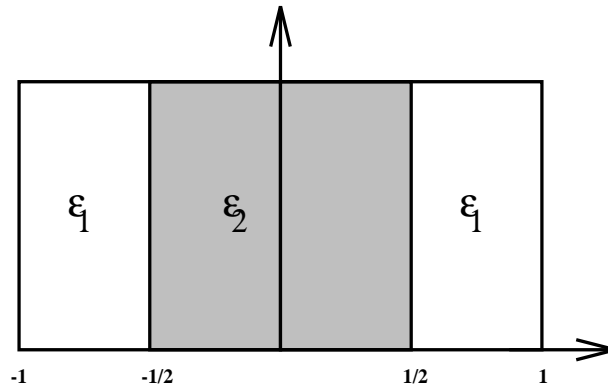


FIG. 4.3. The computational domain

Since E_z is continuous while its second derivatives are discontinuous we use the following fourth-order explicit interpolation to implement the discontinuous dielectric properties in the explicit(2,4) scheme. Define

$$(4.1) \quad A_{int} = \frac{1}{16} \begin{bmatrix} 5 & 15 & -5 & 1 & 0 & \cdot & 0 \\ -1 & 9 & 9 & -1 & \cdot & \cdot & 0 \\ 0 & -1 & 9 & 9 & -1 & \cdot & 0 \\ \cdot & \cdot & \cdot & \cdot & \cdot & \cdot & \cdot \\ 0 & \cdot & \cdot & -1 & 9 & 9 & -1 \\ 0 & \cdot & \cdot & 1 & -5 & 15 & 5 \end{bmatrix}.$$

Then

$$\begin{bmatrix} \epsilon_1 \\ \epsilon_2 \\ \cdot \\ \epsilon_{p-2} \\ \epsilon_{p-1} \end{bmatrix} = A_{int} \begin{bmatrix} \epsilon_{1/2} \\ \epsilon_{3/2} \\ \cdot \\ \cdot \\ \epsilon_{p-1/2} \end{bmatrix}.$$

In two dimensions this is replaced by:

$$[\epsilon_{i,j}] = \frac{1}{2} (A_{int}[\epsilon_{i+1/2,j}] + [\epsilon_{i,j+1/2}]A_{int}^t).$$

For the Yee scheme we take $\epsilon_{interface} = \frac{\epsilon_1 + \epsilon_2}{2}$. An exact solution in this case is:

$$E_z = \begin{cases} 2 \cos(\frac{2\pi}{3}X) \cos(\omega t) \sin(K_y Y) & |X| \leq \frac{1}{2} \quad 0 \leq Y \leq 1 \\ \exp(\frac{\pi\sqrt{3}}{3}) \exp(-\frac{2\pi\sqrt{3}}{3}|X|) \cos(\omega t) \sin(K_y Y) & |X| \geq \frac{1}{2} \quad 0 \leq Y \leq 1 \end{cases}$$

$$H_y = \begin{cases} -\sqrt{\epsilon_2 - \epsilon_1} \sin(\frac{2\pi}{3}X) \sin(\omega t) \sin(K_y Y) & |X| \leq \frac{1}{2} \quad 0 \leq Y \leq 1 \\ -\frac{\sqrt{3(\epsilon_2 - \epsilon_1)}}{2} \exp(\frac{\pi\sqrt{3}}{3}) \exp(-\frac{2\pi\sqrt{3}}{3}X) \sin(\omega t) \sin(K_y Y) & X \geq \frac{1}{2} \quad 0 \leq Y \leq 1 \\ \frac{\sqrt{3(\epsilon_2 - \epsilon_1)}}{2} \exp(\frac{\pi\sqrt{3}}{3}) \exp(\frac{2\pi\sqrt{3}}{3}X) \sin(\omega t) \sin(K_y Y) & X \leq -\frac{1}{2} \quad 0 \leq Y \leq 1 \end{cases}$$

$$H_x = \begin{cases} -\sqrt{\epsilon_1 + 3\epsilon_2} \cos(\frac{2\pi}{3}X) \sin(\omega t) \cos(K_y Y) & |X| \leq \frac{1}{2} \quad 0 \leq Y \leq 1 \\ -\frac{\sqrt{\epsilon_1 + 3\epsilon_2}}{2} \exp(\frac{\pi\sqrt{3}}{3}) \exp(-\frac{2\pi\sqrt{3}}{3}|X|) \sin(\omega t) \cos(K_y Y) & |X| \geq \frac{1}{2} \quad 0 \leq Y \leq 1 \end{cases}$$

where $K_y = \frac{2\pi}{3} \sqrt{\frac{\epsilon_1 + 3\epsilon_2}{\epsilon_2 - \epsilon_1}}$ and $\omega = \frac{4\pi}{3\sqrt{\epsilon_2 - \epsilon_1}}$. Here we choose $\epsilon_1 = 1$ and $\epsilon_2 = 2, 4$. We use the same mesh sizes as before. In Figures 4.4 and 4.5 we draw the errors as a function of the mesh size for various ϵ_2 .

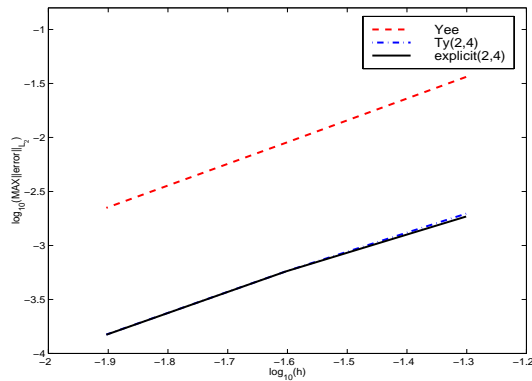


FIG. 4.4. The maximal errors in L_2 norm as a function of the mesh size with $\epsilon_2 = 2$.

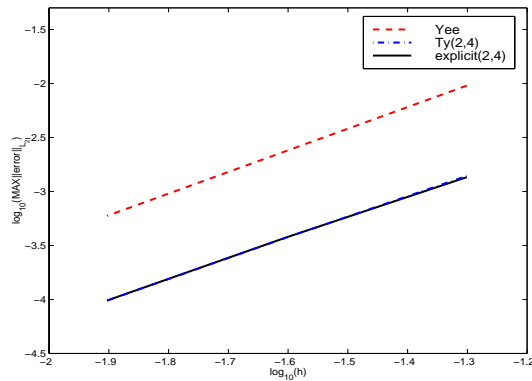


FIG. 4.5. The maximal errors in L_2 norm as a function of the mesh size with $\epsilon_2 = 4$.

Although we get only second order accuracy for the explicit(2,4) scheme we still get much better results

TABLE 4.3
The maximal errors in L_2 norm with $\epsilon_2 = 2$.

<i>scheme</i>	<i>h</i>	Δt	$Max(\ error\ _{L_2})$ $0 \leq t \leq 10$	<i>rate</i>
<i>explicit</i> (2, 4)	$\frac{1}{20}$	$\frac{1}{400}$	0.0019	
<i>explicit</i> (2, 4)	$\frac{1}{40}$	$\frac{1}{1600}$	5.7585×10^{-4}	1.715
<i>explicit</i> (2, 4)	$\frac{1}{80}$	$\frac{1}{3200}$	1.4909×10^{-4}	1.94
<i>Ty</i> (2, 4)	$\frac{1}{20}$	$\frac{1}{400}$	0.00196	
<i>Ty</i> (2, 4)	$\frac{1}{40}$	$\frac{1}{1600}$	5.7721×10^{-4}	1.763
<i>Ty</i> (2, 4)	$\frac{1}{80}$	$\frac{1}{6400}$	1.4955×10^{-4}	1.948
<i>Yee</i>	$\frac{1}{20}$	$\frac{1}{30}$	0.0363	
<i>Yee</i>	$\frac{1}{40}$	$\frac{1}{60}$	0.0089	2.028
<i>Yee</i>	$\frac{1}{80}$	$\frac{1}{120}$	0.00222	2.003

TABLE 4.4
The maximal errors in L_2 norm with $\epsilon_2 = 4$.

<i>scheme</i>	<i>h</i>	Δt	$Max(\ error\ _{L_2})$ $0 \leq t \leq 10$	<i>rate</i>
<i>explicit</i> (2, 4)	$\frac{1}{20}$	$\frac{1}{400}$	0.0014	
<i>explicit</i> (2, 4)	$\frac{1}{40}$	$\frac{1}{1600}$	3.765×10^{-4}	1.894
<i>explicit</i> (2, 4)	$\frac{1}{80}$	$\frac{1}{3200}$	9.7748×10^{-5}	1.945
<i>Ty</i> (2, 4)	$\frac{1}{20}$	$\frac{1}{400}$	0.00139	
<i>Ty</i> (2, 4)	$\frac{1}{40}$	$\frac{1}{1600}$	3.756×10^{-4}	1.887
<i>Ty</i> (2, 4)	$\frac{1}{80}$	$\frac{1}{6400}$	9.7579×10^{-5}	1.944
<i>Yee</i>	$\frac{1}{20}$	$\frac{1}{30}$	0.0095	
<i>Yee</i>	$\frac{1}{40}$	$\frac{1}{60}$	0.00237	2.003
<i>Yee</i>	$\frac{1}{80}$	$\frac{1}{120}$	5.9442×10^{-4}	1.9953

than the ones we get employing the Yee scheme. However, we are using a fourth-order scheme and the loss of two orders of convergence in the presence of heterogeneous dielectrics is undesirable.

An innovative approach to handle heterogeneous dielectrics for the Yee scheme is presented in [6]-[7]. We have extended this approach to include heterogeneous piecewise constant dielectric properties in the explicit(2,4) scheme. As we see below, the fourth-order convergence is recovered globally. We divide the computational domain into three subdomains. Two contain air and the third one contains the lossless dielectric. On the interfaces both the electric and magnetic fields are approximated as follows. Suppose the interfaces are located at $i = I_1$ and $i = I_2$, and $\epsilon = \epsilon_2$ for $I_1 < i < I_2$ while $\epsilon = \epsilon_1$ for $i > I_2$ and $i < I_1$. We approximate H_y at $i = I_1$ and $i = I_2$ by using the following fifth-order extrapolation:

$$\begin{aligned}
 H_{y_{I_1,j}}^{n+1/2} &= \frac{315}{128} H_{y_{I_1-1/2,j}}^{n+1/2} - \frac{105}{32} H_{y_{I_1-3/2,j}}^{n+1/2} + \frac{189}{64} H_{y_{I_1-5/2,j}}^{n+1/2} - \frac{45}{32} H_{y_{I_1-7/2,j}}^{n+1/2} + \frac{35}{128} H_{y_{I_1-9/2,j}}^{n+1/2} \\
 H_{y_{I_2,j}}^{n+1/2} &= \frac{315}{128} H_{y_{I_2+1/2,j}}^{n+1/2} - \frac{105}{32} H_{y_{I_2+3/2,j}}^{n+1/2} + \frac{189}{64} H_{y_{I_2+5/2,j}}^{n+1/2} - \frac{45}{32} H_{y_{I_2+7/2,j}}^{n+1/2} + \frac{35}{128} H_{y_{I_2+9/2,j}}^{n+1/2}
 \end{aligned}$$

$H_{y_{I_1,j}}^{n+1/2}$ can be extrapolated by using the points to the left of I_1 , or by using the points to the right of I_2 because H_y is a continuous function. Once H_y is approximated on the interface we approximate the x-derivative of H_y using $H_{y_{I_1,j}}$ and $H_{y_{I_2,j}}$ as follows:

$$\begin{aligned}\frac{\partial}{\partial x} H_{y_{I_1,j}}^{n+1/2} &\sim \frac{352}{105} H_{y_{I_1,j}} - \frac{35}{8} H_{y_{I_1+1/2}} + \frac{35}{24} H_{y_{I_1+3/2,j}} - \frac{21}{40} H_{y_{I_1+5/2,j}} + \frac{5}{46} H_{y_{I_1+7/2,j}} \\ \frac{\partial}{\partial x} H_{y_{I_2,j}}^{n+1/2} &\sim -\frac{352}{105} H_{y_{I_2,j}} + \frac{35}{8} H_{y_{I_2-1/2}} - \frac{35}{24} H_{y_{I_2-3/2,j}} + \frac{21}{40} H_{y_{I_2-5/2,j}} - \frac{5}{46} H_{y_{I_2-7/2,j}}\end{aligned}$$

Since we discretize the time we want to lose as little information as possible. Therefore, we approximate $\frac{\partial}{\partial x} H_{y_{I_1,j}}^{n+1/2}$ where E_z moves more slowly, i.e. where $\epsilon = \epsilon_2$. Once $\frac{\partial}{\partial x} H_{y_{I_1,j}}^{n+1/2}$ and $\frac{\partial}{\partial x} H_{y_{I_2,j}}^{n+1/2}$ are calculated we can evaluate $EZ_{I_1,j}^{n+1}$ and $EZ_{I_2,j}^{n+1}$ the following way:

$$\begin{aligned}EZ_{I_1,j}^{n+1} &= EZ_{I_1,j}^n - \frac{\Delta t}{24\Delta y} \left(H_{x_{I_1,j-3/2}} - 27H_{x_{I_1,j-1/2}} + 27H_{x_{I_1,j+1/2}} - H_{x_{I_1,j+3/2}} \right) \\ &+ \frac{\Delta t}{\Delta x} \left(\frac{352}{105} H_{y_{I_1,j}}^{n+1/2} - \frac{35}{8} H_{y_{I_1+1/2,j}}^{n+1/2} + \frac{35}{24} H_{y_{I_1+3/2,j}}^{n+1/2} - \frac{21}{40} H_{y_{I_1+5/2,j}}^{n+1/2} + \frac{5}{46} H_{y_{I_1+7/2,j}}^{n+1/2} \right)\end{aligned}$$

Since $\frac{\partial}{\partial x} H_{y_{I_1,j}}^{n+1/2}$ and $\frac{\partial}{\partial x} H_{y_{I_2,j}}^{n+1/2}$ are approximated where $\epsilon = \epsilon_2$ we set $\epsilon = \epsilon_2$ at $i = I_1$ and $i = I_2$. $\frac{\partial}{\partial x} H_{y_{I_1,j}}^{n+1/2}$ is approximated by using points, which are on the right-hand side of I_1 . This is done because the velocity of the waves is $\sqrt{\frac{1}{\epsilon_2}}$ which is smaller than the velocity on the left-hand side of I_1 .

In Figures 4.6a-4.6c we draw the error of the three schemes for various mesh sizes with $\epsilon_2 = 2$ and in Fig 4.7a-4.7c we draw the error of the three schemes for various mesh sizes with $\epsilon_2 = 4$. In Fig 4.6d and 4.7d we draw the errors as a function of the mesh size. The slope of the Yee scheme is 2 and the slope of the Ty(2,4) scheme and the explicit(2,4) converges to 4 as can also be seen in table 4.5 and table 4.6.

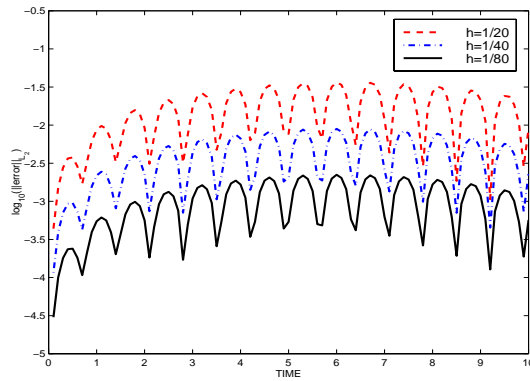


FIG. 4.6A. $\log_{10}(\|error\|_{L_2})$ For the Yee scheme.

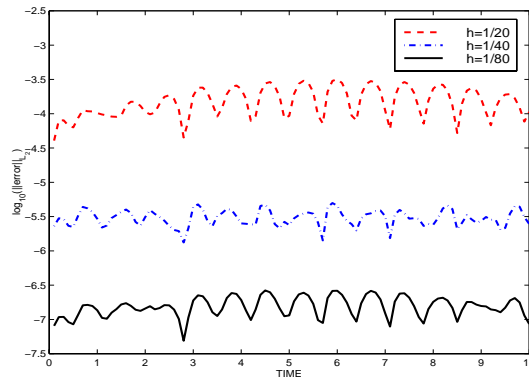


FIG. 4.6B. $\log_{10}(\|error\|_{L_2})$ for the explicit(2,4) scheme.

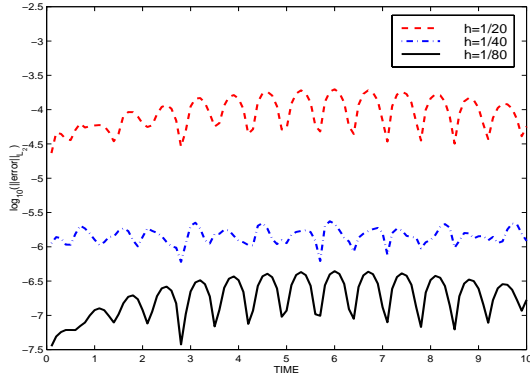


FIG. 4.6C. $\log_{10}(\|error\|_{L_2})$ for the $Ty(2,4)$ scheme.

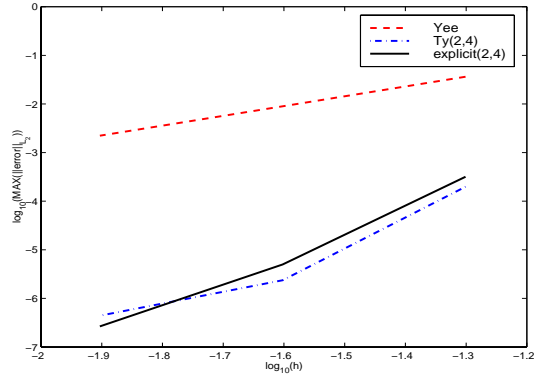


FIG. 4.6D. $\log_{10}(\|error\|_{L_2})$ as a function of $\log_{10}(h)$ For the Yee, the explicit(2,4) and the $Ty(2,4)$ schemes.

TABLE 4.5

The maximal errors in L_2 norm with $\epsilon_2 = 2$.

<i>scheme</i>	<i>h</i>	Δt	$Max(\ error\ _{L_2})$ $0 \leq t \leq 10$	<i>rate</i>
<i>explicit(2,4)</i>	$\frac{1}{20}$	$\frac{1}{400}$	3.1829×10^{-4}	
<i>explicit(2,4)</i>	$\frac{1}{40}$	$\frac{1}{1600}$	4.9839×10^{-6}	5.996
<i>explicit(2,4)</i>	$\frac{1}{80}$	$\frac{1}{3200}$	2.6518×10^{-7}	4.23
<i>Ty(2,4)</i>	$\frac{1}{20}$	$\frac{1}{400}$	1.978×10^{-4}	
<i>Ty(2,4)</i>	$\frac{1}{40}$	$\frac{1}{1600}$	2.3593×10^{-6}	6.389
<i>Ty(2,4)</i>	$\frac{1}{80}$	$\frac{1}{6400}$	4.4066×10^{-7}	2.420
<i>Yee</i>	$\frac{1}{20}$	$\frac{1}{30}$	0.0363	
<i>Yee</i>	$\frac{1}{40}$	$\frac{1}{60}$	0.0089	2.028
<i>Yee</i>	$\frac{1}{80}$	$\frac{1}{120}$	0.00222	2.003

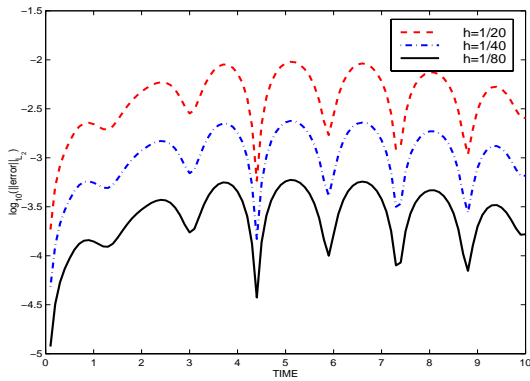


FIG. 4.7A. $\log_{10}(\|error\|_{L_2})$ For the Yee scheme.

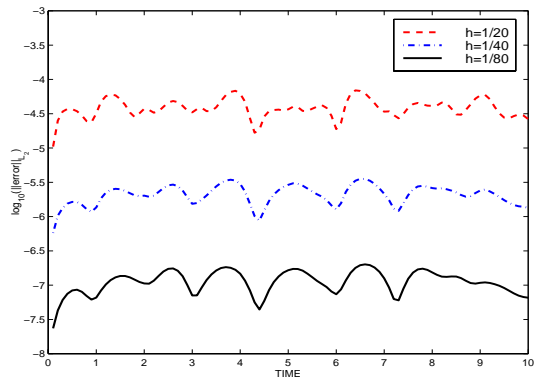


FIG. 4.7B. $\log_{10}(\|error\|_{L_2})$ for the explicit(2,4) scheme.

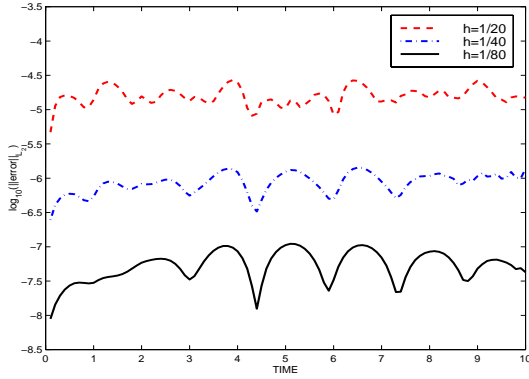


FIG. 4.7C. $\log_{10}(\|error\|_{L_2})$ for the $Ty(2,4)$ scheme.

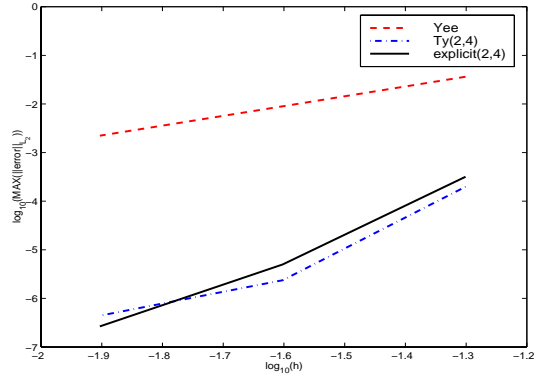


FIG. 4.7D. $\log_{10}(\|error\|_{L_2})$ as a function of $\log_{10}(h)$ For the Yee, the explicit(2,4) and the $Ty(2,4)$ schemes.

TABLE 4.6
The maximal errors in L_2 norm with $\epsilon_2 = 4$.

<i>scheme</i>	h	Δt	$Max(\ error\ _{L_2})$ $0 \leq t \leq 10$	<i>rate</i>
<i>explicit(2,4)</i>	$\frac{1}{20}$	$\frac{1}{400}$	6.9239×10^{-5}	
<i>explicit(2,4)</i>	$\frac{1}{40}$	$\frac{1}{1600}$	3.5486×10^{-6}	4.286
<i>explicit(2,4)</i>	$\frac{1}{80}$	$\frac{1}{3200}$	2.0112×10^{-7}	4.141
<i>Ty(2,4)</i>	$\frac{1}{20}$	$\frac{1}{400}$	2.7043×10^{-5}	
<i>Ty(2,4)</i>	$\frac{1}{40}$	$\frac{1}{1600}$	1.4233×10^{-6}	4.249
<i>Ty(2,4)</i>	$\frac{1}{80}$	$\frac{1}{6400}$	1.1040×10^{-7}	3.688
<i>Yee</i>	$\frac{1}{20}$	$\frac{1}{30}$	0.0095	
<i>Yee</i>	$\frac{1}{40}$	$\frac{1}{60}$	0.00237	2.003
<i>Yee</i>	$\frac{1}{80}$	$\frac{1}{120}$	5.9442×10^{-4}	1.9953

Next, we look at a coated perfect conductor with a dielectric layer. The coating thickness is $\frac{1}{2}$ with a relative permittivity of ϵ_2 as shown in Fig 4.8 .

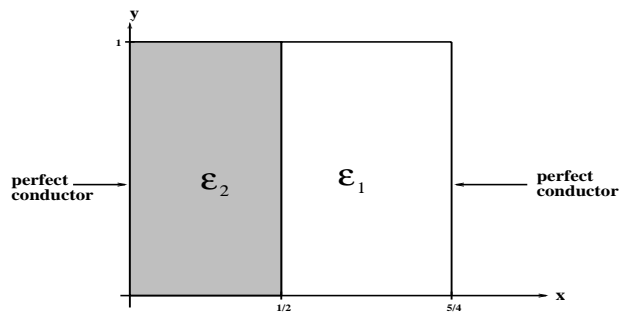


FIG. 4.8. The computational domain

We take $\epsilon_2 = 2$ and $\epsilon_1 = 1$. An exact solution in this case can be:

$$E_z = \begin{cases} \sin(a_1 X) \sin(\omega t) \sin(bY) & 0 \leq X \leq \frac{1}{2} & 0 \leq Y \leq 1 \\ \cos(a_2 X) \sin(\omega t) \sin(bY) & \frac{1}{2} \leq X \leq \frac{5}{4} & 0 \leq Y \leq 1 \end{cases}$$

$$H_y = \begin{cases} -\frac{a_1}{\omega} \cos(a_1 X) \cos(\omega t) \sin(bY) & 0 \leq X \leq \frac{1}{2} & 0 \leq Y \leq 1 \\ \frac{a_2}{\omega} \cos(a_2 X) \cos(\omega t) \sin(bY) & \frac{1}{2} \leq X \leq \frac{5}{4} & 0 \leq Y \leq 1 \end{cases}$$

$$H_x = \begin{cases} \frac{b}{\omega} \sin(a_1 X) \cos(\omega t) \cos(bY) & 0 \leq X \leq \frac{1}{2} & 0 \leq Y \leq 1 \\ \frac{b}{\omega} \sin(a_2 X) \cos(\omega t) \cos(bY) & \frac{1}{2} \leq X \leq \frac{5}{4} & 0 \leq Y \leq 1 \end{cases}$$

where

$$a_1^2 + b^2 = \epsilon_2 \omega^2$$

$$a_2^2 + b^2 = \epsilon_1 \omega^2$$

$$x = \frac{1}{2} : \sin\left(\frac{a_1}{2}\right) = \cos\left(\frac{a_2}{2}\right)$$

$$x = \frac{5}{4} : \cos\left(\frac{5a_2}{4}\right) = 0$$

We choose:

$$\epsilon_1 = 1$$

$$\epsilon_2 = 2$$

$$a_1 = 3\pi$$

$$a_2 = 2\pi$$

$$b = \pi$$

$$\omega = \sqrt{5}\pi$$

On the interface between the air and the dielectric we use the same technique we used in the previous example. In Figures 4.9a-4.9c we draw the errors for various mesh sizes. In Figure 4.9d we draw the errors as a function of the mesh size. For the Yee scheme we get second order accuracy and for the Ty(2,4) and the explicit(2,4) the accuracy converges to 4, which can also be seen in Table 4.7.

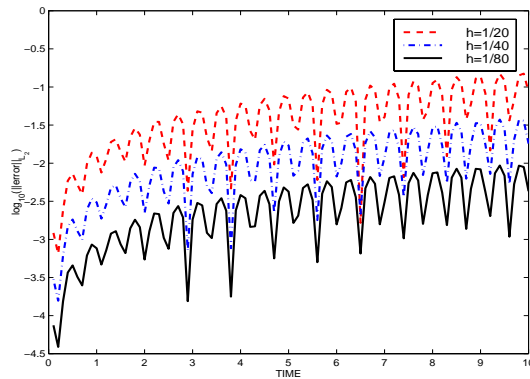


FIG. 4.9A. $\log_{10}(\|error\|_{L_2})$ For the Yee scheme.

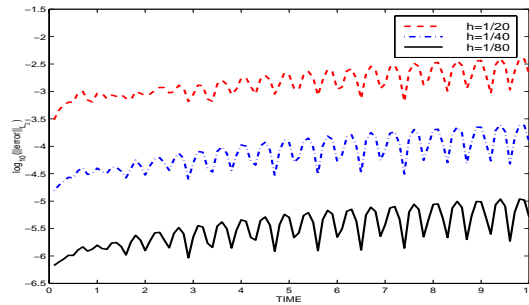


FIG. 4.9B. $\log_{10}(\|error\|_{L_2})$ for the explicit(2,4) scheme.

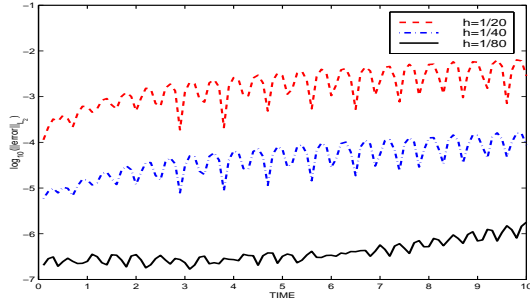


FIG. 4.9C. $\log_{10}(\|error\|_{L_2})$ for the $Ty(2,4)$ scheme.

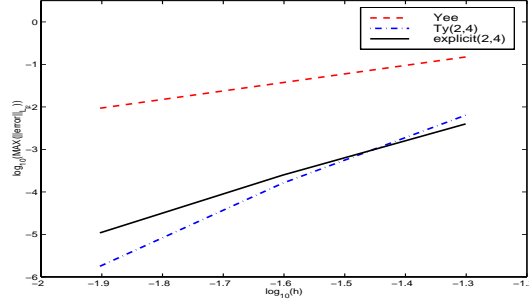


FIG. 4.9D. $\text{Log}_{10}(\|error\|_{L_2})$ as a function of $\text{Log}_{10}(h)$ For the Yee, the explicit(2,4) and the $Ty(2,4)$ schemes.

TABLE 4.7
The maximal errors in L_2 norm .

scheme	h	Δt	$Max(\ error\ _{L_2})$ $0 \leq t \leq 10$	rate
explicit(2,4)	$\frac{1}{20}$	$\frac{1}{400}$	0.00398	
explicit(2,4)	$\frac{1}{40}$	$\frac{1}{1600}$	2.4868×10^{-4}	4.001
explicit(2,4)	$\frac{1}{80}$	$\frac{1}{3200}$	1.0889×10^{-5}	4.513
$Ty(2,4)$	$\frac{1}{20}$	$\frac{1}{400}$	0.0063	
$Ty(2,4)$	$\frac{1}{40}$	$\frac{1}{1600}$	1.609×10^{-4}	5.308
$Ty(2,4)$	$\frac{1}{80}$	$\frac{1}{6400}$	1.7820×10^{-6}	6.497
Yee	$\frac{1}{20}$	$\frac{1}{30}$	0.1498	
Yee	$\frac{1}{40}$	$\frac{1}{60}$	0.037	2.004
Yee	$\frac{1}{80}$	$\frac{1}{120}$	0.0093	2.0026

To our knowledge, this is the first fourth-order scheme that preserves its convergence rate when discontinuities in the coefficients are present.

Next we consider a monochromatic isotropic point source of wavelength 0.25, that is switched on at $t = 0$ and radiates in free-space. The domain is $0 \leq x, y \leq 1$. For Yee's scheme we choose $h = \frac{1}{40}$, $\Delta t = \frac{2h}{3}$, for the explicit(2,4) and the $Ty(2,4)$ scheme $h = \frac{1}{40}$, $\Delta t = h^2$. The point source is modeled by adding a term representing a current $I_z(t) = 0.01 \sin(8\pi t)\epsilon(t)$ at $(x, y) = (\frac{1}{4}, \frac{1}{4})$ where $\epsilon(t)$ denotes the Heaviside unit-step function. For the pulse under consideration, the radiated field is the solution of

$$(4.2) \quad \partial_x^2 E_z + \partial_y^2 E_z - \partial_t^2 E_z = Z \partial_t I_z(t) \delta(r - r_s)$$

$r - r_s = (x - \frac{1}{4}, y - \frac{1}{4})$. The solution consists of rotationally symmetric outgoing waves. The exact solution is

$$E_z(r, t) = -\frac{Z}{2\pi} \int_0^\infty \frac{\partial_t I_z(t - \sqrt{|(r - r_s)|^2 + \xi^2})}{\sqrt{|(r - r_s)|^2 + \xi^2}} d\xi$$

In Fig. 4.10 we plot the errors, in the L_2 norm, for the various approximate solutions.

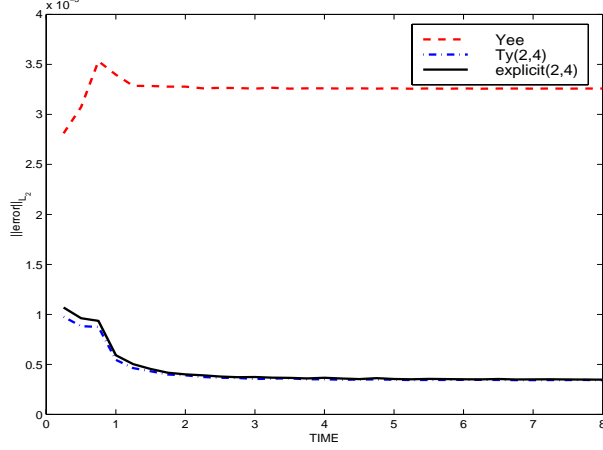


FIG. 4.10. The errors in L_2 norm between the numerical solution and the exact solution of 4.2.

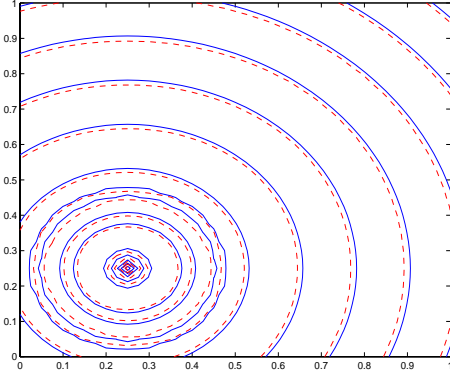


FIG. 4.11. The contours of the Yee scheme and the exact solution at $t = 8$. The Yee scheme is drawn by $--$ and the exact solution is drawn by a solid line.

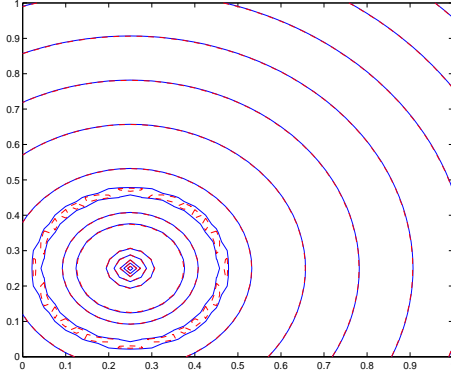


FIG. 4.12. The contours of the explicit(2,4) scheme and the exact solution at $t = 8$. The explicit(2,4) scheme is drawn by $--$ and the exact solution is drawn by a solid line.

Next we consider a monochromatic isotropic point source of wavelength 0.25, that is switched on at $t = 0$ in the presence of an infinite perfect conductor (fig 4.13). The domain is $-\infty \leq x, y \leq \frac{1}{2}$, $-\infty \leq y \leq \infty$. For Yee's scheme we choose $h = \frac{1}{40}$, $\Delta t = \frac{2h}{3}$, for the explicit(2,4) and the Ty(2,4) schemes $h = \frac{1}{40}$, $\Delta t = h^2$. The point source is modeled by adding a term representing a current $I_z(t) = 0.01 \sin(8\pi t)\epsilon(t)$ at $(x, y) = (\frac{1}{4}, \frac{1}{4})$ where $\epsilon(t)$ denotes the Heaviside unit-step function. The equations in this case are:

$$\begin{aligned} \frac{\partial E_z}{\partial t} &= Z \left(\frac{\partial H_y}{\partial x} - \frac{\partial H_x}{\partial y} \right) - Z I_z(t) \delta(r - r_s) \\ \frac{\partial H_x}{\partial t} &= -\frac{1}{Z} \frac{\partial E_z}{\partial y} \\ \frac{\partial H_y}{\partial t} &= \frac{1}{Z} \frac{\partial E_z}{\partial x} \end{aligned}$$

With the boundary conditions:

$$(4.3) \quad E_z(1/2, y, t) = 0$$

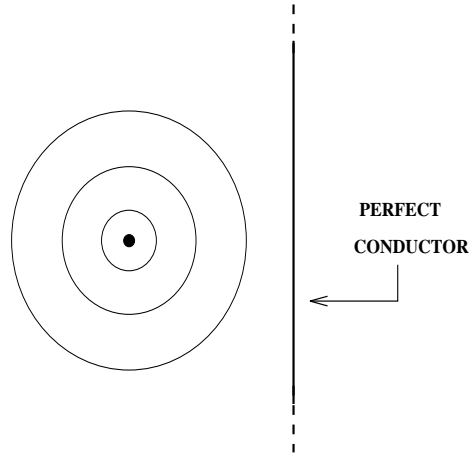


FIG. 4.13. *The computational domain.*

The exact solution can be constructed by using the exact solution for the previous case and by using the image method.

In Figures 4.14, 4.15 and 4.16 we draw the errors in L_2 norm and the contours of the exact and numerical solutions.

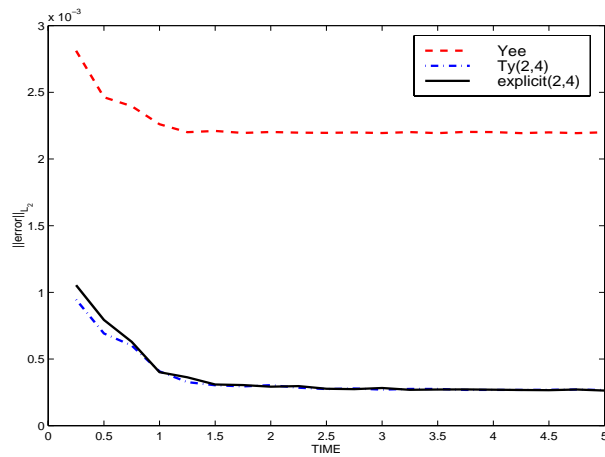


FIG. 4.14. *The errors in L_2 norm between the numerical solutions and the exact solution of 4.3.*

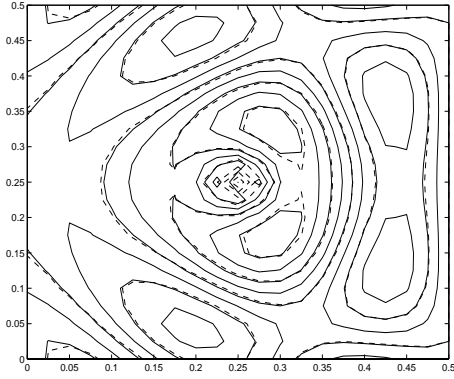


FIG. 4.15. The contours of the Yee scheme and the exact solution at $t = 5$. The Yee scheme is drawn by $--$ and the exact solution is drawn by a solid line

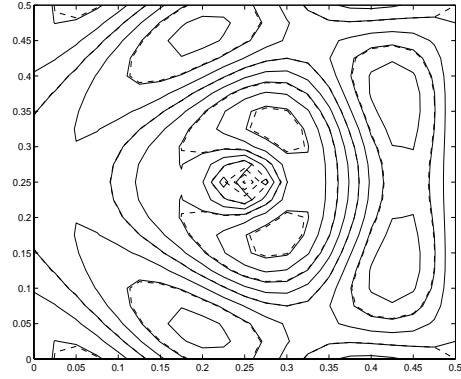


FIG. 4.16. The contours of the explicit(2,4) scheme and the exact solution at $t = 5$. The explicit(2,4) scheme is drawn by $--$ and the exact solution is drawn by a solid line.

Next we consider a monochromatic pointsource in the presence of an inclined perfect conductor Fig 4.17a . We test these three schemes by using the staircasing method. We meshure the error in L_1 norm along the dashed line which can be seen in Fig 4.17b . As can be seen from Fig 4.17c the Ty(2,4) scheme is unstable whereas the Yee scheme and the explicit(2,4) schemes are stable. In [9] the Ty(2,4) scheme was tested as well but there the Ty(2,4) scheme was stable.

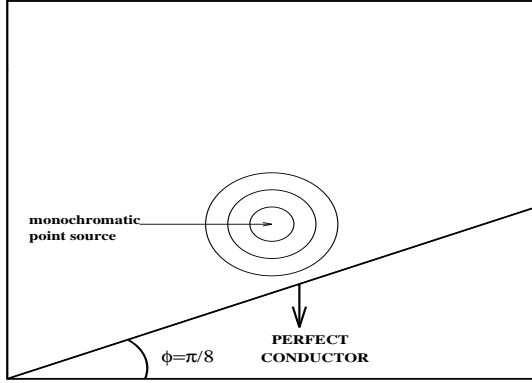


FIG. 4.17A. Computational domain.

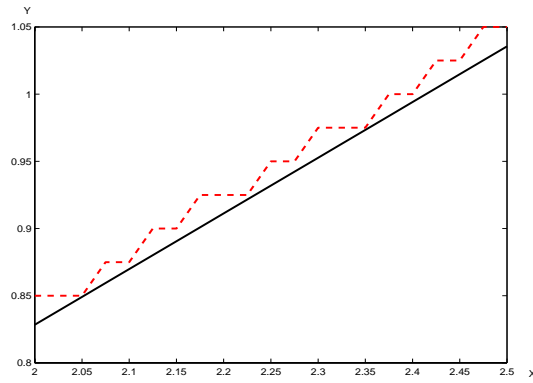


FIG. 4.17B. Location of the grid points.

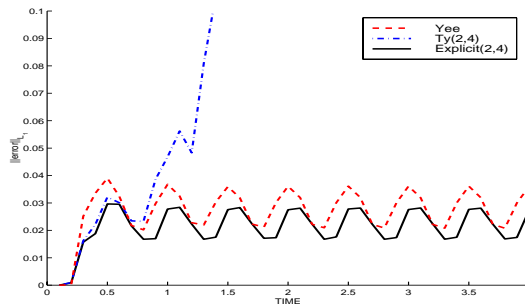


FIG. 4.17C. The $\|error\|_{L_1}$ as a function of time for the Yee, the explicit(2,4) and the Ty(2,4) schemes.

Next we test these three schemes in $[0, 1/2] \times [0, 1/4] \times [0, 1/2]$ domain. An exact solution in this case can be [8]:

$$\begin{aligned}
 H_x &= \sin(\omega t) \sin(Ax + By + Cz) \\
 H_y &= \sin(\omega t) \sin(Ax + By + Cz) \\
 H_z &= \sin(\omega t) \sin(Ax + By + Cz) \\
 E_x &= \frac{C - B}{\omega} \cos(\omega t) \cos(Ax + By + Cz) \\
 E_y &= \frac{A - C}{\omega} \cos(\omega t) \cos(Ax + By + Cz) \\
 E_z &= \frac{B - A}{\omega} \cos(\omega t) \cos(Ax + By + Cz)
 \end{aligned}$$

Where

$$\begin{aligned}
 \omega^2 &= A^2 + B^2 + C^2 \\
 0 &= A + B + C
 \end{aligned}$$

We choose:

$$\begin{aligned}
 A &= \pi \\
 B &= -2\pi \\
 C &= \pi \\
 \omega &= \sqrt{6}\pi
 \end{aligned}$$

In table 4.8, we can see that for the explicit(2,4) and the Ty(2,4) schemes we have used $\Delta t = h^2$ and for the Yee scheme we have used $\Delta t = \frac{4h}{7}$. The explicit(2,4) as well as the Ty(2,4) schemes behave better than expected and gives almost fifth order of accuracy.

For all this cases we have measured the error between the approximated electric field in the z direction and the exact electric field in the z direction in L_2 norm.

TABLE 4.8
Comparison of the errors in L_2 norm

<i>scheme</i>	<i>h</i>	Δt	$Max(\ error\ _{L_2})$ $0 \leq t \leq 10$	rate
<i>explicit(2, 4)</i>	$\frac{1}{20}$	$\frac{1}{400}$	5.375×10^{-4}	
<i>explicit(2, 4)</i>	$\frac{1}{40}$	$\frac{1}{1600}$	2.184×10^{-5}	4.621
<i>explicit(2, 4)</i>	$\frac{1}{80}$	$\frac{1}{3200}$	9.071×10^{-7}	4.590
<i>Ty(2, 4)</i>	$\frac{1}{20}$	$\frac{1}{400}$	3.621×10^{-4}	
<i>Ty(2, 4)</i>	$\frac{1}{40}$	$\frac{1}{1600}$	1.144×10^{-5}	4.983
<i>Ty(2, 4)</i>	$\frac{1}{80}$	$\frac{1}{6400}$	3.5621×10^{-7}	5.005
<i>Yee</i>	$\frac{1}{20}$	$\frac{1}{35}$	0.0027	
<i>Yee</i>	$\frac{1}{40}$	$\frac{1}{70}$	7.3×10^{-4}	1.9028
<i>Yee</i>	$\frac{1}{80}$	$\frac{1}{140}$	1.8252×10^{-4}	2.0015

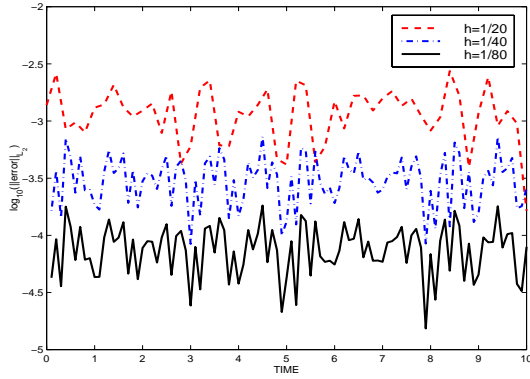


FIG. 4.18A. $\log_{10}(\|error\|_{L_2})$ for the Yee scheme.

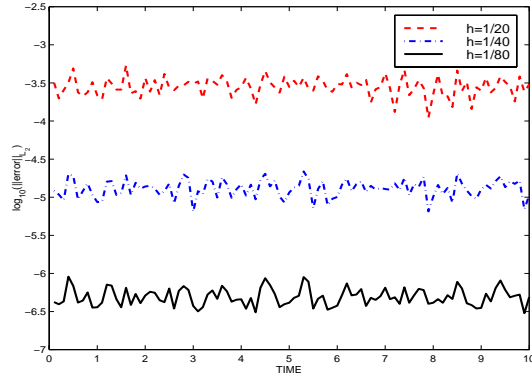


FIG. 4.18B. $\log_{10}(\|error\|_{L_2})$ for the explicit(2,4) scheme.

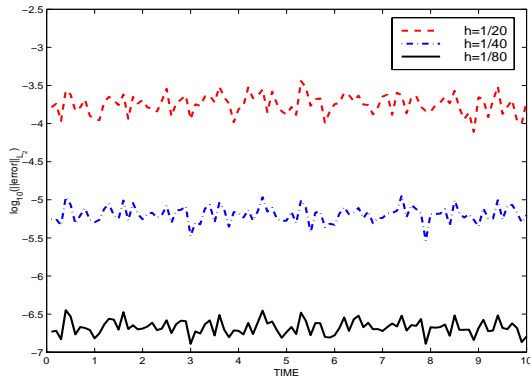


FIG. 4.18C. $\log_{10}(\|error\|_{L_2})$ for the Ty(2,4) scheme.

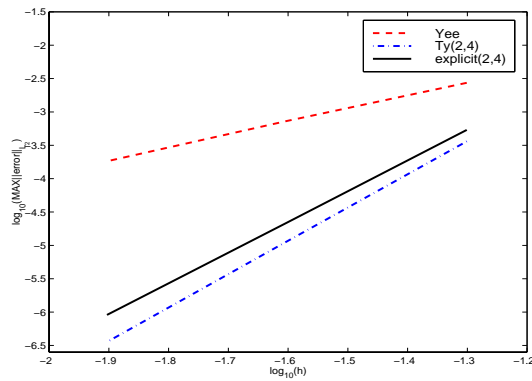


FIG. 4.18D. $\log_{10}(\|error\|_{L_2})$ as a function of $\log_{10}(h)$ For the Yee, the explicit(2,4) and the Ty(2,4) schemes.

5. Computational Cost Comparisons. In order to compare the efficiency of the explicit(2,4), the Ty(2,4) and Yee scheme we examine the following boundary conditions:

$$\begin{aligned}
 E_z &= \sin(3\pi x) \sin(4\pi y) \\
 H_y &= (3/5) \cos(3\pi x) \sin(4\pi y) \sin\left(\frac{5\pi\Delta t}{2}\right) \\
 H_x &= -(4/5) \sin(3\pi x) \cos(4\pi y) \sin\left(\frac{5\pi\Delta t}{2}\right)
 \end{aligned}$$

The exact solution in this case is:

$$E_z = \sin(3\pi x) \sin(4\pi y) \cos(5\pi t)$$

For the Ty(2,4) scheme and the explicit(2,4) scheme we use a uniform gridspacing with $\Delta x = \Delta y = \frac{1}{30}$. For the Yee scheme we also use uniform gridspacing with $\Delta x = \Delta y = \frac{1}{240}$. We chose these mesh sizes in order to get the same error between the exact E_z and the approximated E_z in L_2 norm. The comparison is shown in table 5.1. The programs were written in fortran and run on a Digital Alpha workstation.

The CPU time needed to achieve the same accuracy in Yee's case is more than 11 times larger than required for the Ty(2,4) scheme and 91 times larger than required for the explicit(2,4) scheme.

TABLE 5.1
CPU-time using various difference schemes.

<i>scheme</i>	h	Δt	$Max(\ error\ _{L_2})$ $0 \leq t \leq 10$	<i>CPU - time</i>
<i>explicit(2,4)</i>	$\frac{1}{30}$	$\frac{1}{900}$	1.99×10^{-3}	0.9 sec
<i>Ty(2,4)</i>	$\frac{1}{30}$	$\frac{1}{900}$	1.25×10^{-3}	5.7 sec
<i>Yee</i>	$\frac{1}{240}$	$\frac{1}{360}$	1.31×10^{-3}	91sec

6. Discussion and Conclusion. The results demonstrate that we can use a coarser mesh with the fourth order scheme and still get the same accuracy as with the Yee scheme. This is true even in the presence of a dielectric media.

Although this scheme is not as good as the Ty(2,4) scheme[2], it is still easier to modify an existing code based on the Yee scheme and make it fourth order accurate, by using the explicit(2,4) scheme. This is true because in the Ty(2,4) scheme one has to inverse a matrix by using a LU decomposition.

REFERENCES

- [1] K.S. YEE, *Numerical Solution of Initial Boundary Value Problems Involving Maxwell's Equation in Isotropic Media*, *IEEE Transactions on Antennas and Propagation*, v. AP-14, 1966, pp. 302-307.
- [2] E. TURKEL AND A. YEFET, *Fourth Order Accurate Compact Implicit Method for the Maxwell Equations*, submitted to *IEEE Transactions on Antennas and Propagation*.
- [3] H.O. KREISS AND J. OLIGER, "Comparison of Accurate Methods for the Integration of Hyperbolic Equations," *Tellus* v. 24,1972, pp. 199-215.
- [4] A. TAFLOVE, *Computational Electrodynamics: The Finite-Difference Time-Domain Method*, Artech House, 1996.
- [5] D. GOTTLIEB AND B. YANG, *Comparisons of Staggered and Non-Staggered Schemes for Maxwell's Equations*, *12th Annual Review of Progress in Applied Computational Electromagnetics*, 1996.
- [6] K. H. DRIDI, J. S. HESTHAVEN AND A. DITKOWSKI, *Staircase Free Finite-Difference Time-Domain Formulation for Arbitrary Material Distributions in General Geometries*, submitted to *IEEE Transactions on Antennas and Propagation*.
- [7] A. DITKOWSKI AND J. S. HESTHAVEN. PRIVATE COMMUNICATION.
- [8] A. YEFET AND E. TURKEL, *Construction of Three Dimensional Solutions for the Maxwell Equations*, *NASA/CR-1998-208954 ICASE Interim Report No. 34*.
- [9] S. ABARBANEL, A. DITKOWSKI AND A. YEFET, *Bounded Error Schemes for the Wave Equation on Complex Domains*, *NASA/CR-1998-208740 ICASE Report No. 98-50*.
- [10] P.G. PETROPOULOS, *Phase Error Control for FD-TD Methods of Second and Fourth Order Accuracy*, *IEEE Transaction on Antennas and Propagation*, v. 42, NO. 6, 1994, PP. 859-862.
- [11] C.W. MANRY, S.L. BROCHAT AND J.B. SCNEIDER, *Higher-Order FDTD Methods for Large Problems*, *J. Applied Computational Electromagnetics Society*, v. 10, NO. 2, 1995, PP. 17-29.
- [12] J. FANG, *Time Domain Finite Difference Computation for Maxwell's Equations*, *PhD. Dissertation, University of California at Berkeley*, 1989.
- [13] A. NACHMAN, *A Brief Perspective on Computational Electromagnetics*, *J. Computational Physics*, v. 129, 1996, PP. 237-240.

- [14] P.G. PETROPOULOS, L. ZHAO AND A.C. CANGELLARIS, *A Reflectionless Sponge Layer Absorbing Boundary Condition for the Solution of Maxwell's Equations with High-Order Staggered Finite Difference Schemes*, *J. Computational Physics*, v. 139, 1998 pp. 184-208.
- [15] Y. LIU, *Fourier Analysis of Numerical Algorithms for the Maxwell Equations*, *J. Computational Physics*, v. 124, 1996, pp. 396-406.